RSC Advances

ROYAL SOCIETY OF CHEMISTRY

www.rsc.org/advances

An abnormal phase transition behavior in VO_2 nanoparticles induced by a M1-M2-R process: two anomalous high (> 68 °C) transition temperatures

Bingrong Dong,[1] Nan Shen,[1] Chuanxiang Cao,[1] Zhang Chen,[2] Hongjie Luo,[1,2] Yanfeng Gao,[2,3]*

1 State Key Laboratory of High Performance Ceramics and Superfine Microstructure, Shanghai institute of Ceramics, Chinese Academy of Sciences, 1295 Dingxi, Shanghai 200050, China

2 School of Materials Science and Engineering, Shanghai University, 99 Shangda, Shanghai 200444, China

3 Key Laboratory for Palygorskite Science and Applied Technology of Jiangsu Province, Jiangsu Provincial Engineering Laboratory for Advanced Materials of Salt Chemical Industry, Huaiyin Institute of Technology, Huaian 223003, People's Republic of China

* Author for correspondence. Email: yfgao@shu.edu.cn

Tel/Fax: +86-21-6990-6218

Abstract

Vanadium dioxide (VO_2) has a reversible metal–insulator transition (MIT) at 68 °C and can be used to develop thermally and electrically sensible devices. In this work, an abnormal phase transition behavior of VO_2 nanoparticles was discovered according to the comparison of pristine nanoparticles without and with high-temperature thermal treatment. Single phase transition temperature at 65.1 °C for the pristine VO_2 nanoparticles split into two temperatures approximately being located at 74 °C (T_1) and 84 °C (T_2) respectively after thermal treatment at 400 °C for 6 h. Both temperatures are greatly lager than 68 °C. Through the characterization of Raman and transmission electron microscopy (TEM), the two higher transition temperatures could be well explained by the arising of VO_2 (M2). Amounts of grain boundaries were observed during the merger and fusion processes of VO_2 nanoparticles at high temperature. The grain boundaries and interfacial defects resulted in the dislocation of lattice structure, and then produced the stress and strain in VO_2 nanoparticles. Consequently the VO_2 (M2) with a higher temperature formed in the heating process and the initial MIT (M1 – R) became a M1 – M2 – R behavior. Moreover, the thermal treatment improves the phase transition enthalpy (ΔH) of VO_2, which promotes the increase of solar modulation ability (ΔT_{sol}) of VO_2-PET composite film from 12.8 % to 15.2 – 17.0 % without the expense of the luminous transmittance. These findings are of great significance to the deep understanding of MIT and the development of VO_2 smart windows.

Keywords: vanadium dioxide; thermal treatment; phase transition; thermochromic;

1 Introduction

Vanadium dioxide, a strongly correlated electron material, is extremely interesting for exploration of the metal–insulator transition (MIT) as well as various applications. The MIT occurs from a monoclinic (M1), insulating phase at low temperatures to a rutile (R), metallic phase at high temperatures at a critical temperature of 68 °C (341 K), accompanied with remarkable changes in electronic and optical properties[1]. Amounts of applications have been proposed and employed, such as smart window[2, 3], Mott transistor[4], strain sensor[5], gas sensor[6], temperature sensor[7], thermal actuator[8] and so on.

For a series of applications, it is necessary to tailor phase transition temperature (T_{MIT}) to meet different requirements. Thus various methods have been carried out to tune the T_{MIT}. Doping is widely employed to decrease the T_{MIT}, by substitution of V^{4+} with W^{6+}, Mo^{6+}, Mg^{2+}, F^{-} and Nb^{5+}.[9-12] Moreover, the size effect[13] via controlling the size of VO_2 nanoparticles could regulate the MIT of VO_2 and the strain along c_R-axis could increase the T_{MIT} due to the arising of the M2 phase from M1 phase of VO_2[14, 15]. Recent research also found that oxygen vacancies can be employed to tune the T_{MIT} in a wide range[16]. In addition, other impact factors including crystallinity and stoichiometry also have been investigated to regulate the T_{MIT}.[17, 18] Thus, the MIT and the corresponding T_{MIT} of VO_2 are critically influenced by the above factors.

Since VO_2 nanoparticles have different morphologies due to the different hydrothermal conditions, it is complicated to distinguish the effects of those factors on the MIT of VO_2 nanoparticles. Chen et. al[19] prepared fine crystal quality VO_2 nanoparticles via the hydrothermal reaction at high temperatures (300 – 390 °C) and the obtained VO_2 nanoparticles showed an asymmetrical phase transition and increased insulator–metal transition temperatures. The two endothermic peaks located at 68 °C (low MIT peak) and 91 °C (high MIT peak) were observed unexpectedly during the DSC test. This phenomenon was ascribed to the size effect and the shape-dependence, however it was still hard to clearly distinguish the function of the above factors. Li et. al[20] took advantage of the transformation from VO_2 (D) to VO_2

(M1) to obtain VO_2 (M1) nanoparticles via the combination of the hydrothermal synthesis and a subsequent mild thermal treatment at 300 – 450 °C, and found that interfacial defects and the size effect played essential roles in regulating the MIT of VO_2.

In this work, we found an abnormal phase transition process of VO_2 nanoparticles. Namely single peak at 65.1 °C in the phase transition of pristine VO_2 nanoparticles splits into two peaks after thermal treatment at high temperatures (400 – 440 °C) for certain time. Two peaks of samples obtained from annealing at 400 °C for 6 hours are approximately located at 74 °C (the low temperature, T_1) and 84 °C (the high temperature, T_2) respectively, which are both higher than 68 °C for bulk VO_2. The reason for the increased MIT temperatures could be attributed to the arising of VO_2 (M2) and will be explained in detail in this paper. On the other hand, the thermal treatment improves the ΔH of VO_2 and the ΔT_{sol} of VO_2-PET composite film. The ΔT_{sol} increases from 12.8 % to 15.2 – 17.0 % without the expense of luminous transmittance. This study could enhance the understanding of the MIT of VO2 nanoparticles and promote the development of VO_2-PET flexible foil.

2 Experimental Methods

2.1 The preparation of VO_2 (M1) powders

VO_2 nanoparticles were prepared according to a previously reported method[2]. All reagents were purchased from the Sinopharm Chemical Reagent Co., Ltd., and used without further purification. Vanadium pentoxide (V_2O_5, analytically pure) and diamide hydrochloride ($N_2H_4 \cdot HCl$, analytically pure) were employed as starting materials to prepare a VO^{2+} solution. Concentrated HCl (6 mL, 38%) and a solution containing 1 g of $N_2H_4 \cdot HCl$ were added into an aqueous suspension (20 mL) containing 3.5 g of V_2O_5. The solution was treated with a small amount of V_2O_5 or $N_2H_4 \cdot HCl$ until it contained no VO^{2+} or V^{3+} and was then filtered to form a clear VO^{2+} solution (pH ≈ 1). The solution was stirred for 10 min and then transferred to a 50 mL stainless steel autoclave. The hydrothermal reaction was carried out at 260 °C

for 6 h. The final black product was separated by centrifugation, washed with water and ethanol and then dried in a vacuum drying oven at 60 °C for 24 h. The obtained VO_2 (M1) nanoparticles were heated in a tube furnace under a flow of nitrogen gas at 400 – 440 °C for defined time to study the effect of annealing time and annealing temperature.

2.2 Characterization

The morphologies of the resulting powders were analysed via transmission electron microscopy (TEM, JEM2010, JEOL, Japan) and scanning electron microscopy (SEM, Magellan 400), respectively. The crystalline phases of the nanoparticles were determined by X-ray diffraction (XRD, Model D/Max 2550 V, Rigaku, Japan). The phase transition temperatures of the products were measured via differential scanning calorimetry (DSC, DSC200F3, NETZSCH) in nitrogen flow at a heating rate of 10 °C min^{-1}. The Raman spectra of the composite samples were measured using a Raman microscope (Renishaw in Via) with a 514 nm laser source at an input power of 1 mW. The thermochromic properties were evaluated by the VO_2-PET composite films. For measurements, the VO_2 powders were uniformly dispersed in polyurethane after surface modification by poly(vinylpyrrolidone) (PVP), and then deposited on polyethylene terephthalate (PET) via knife-coating, and finally dried at 70 °C. The optical transmittance characteristics were monitored using a Hitachi U-4100 UV-visible-near-IR spectrophotometer equipped with a film heating unit in the wavelength range of 350-2600 nm. For all samples, the integral visible transmittance (T_{lum}, 350 - 750 nm) and solar transmittance (T_{sol}, 240 - 2600 nm) were obtained based on the measured spectra using the following equation:

$$T_i = \int \varphi_i(\lambda) T(\lambda) d\lambda / \int \varphi_i(\lambda) d\lambda \qquad (1)$$

$$\Delta T_{sol} = T_{sol}(T < T_c) - T_{sol}(T > T_c) \qquad (2)$$

where $T(\lambda)$ denotes the transmittance at wavelength λ, i denotes 'lum' or 'sol' for the calculations, T and ΔT_{sol} are the temperature and solar modulation ability, respectively; φ_{lum} is the standard luminous efficiency function for the photopic vision according to CIE 1931 standards, and φ_{sol} is the solar irradiance spectrum for the air mass 1.5

(corresponding to the sun standing 37° above the horizon) according to ASTM G173-03 Reference Spectra.

3 Results and discussion

3.1 The effect of annealing time and temperature to the MIT of VO_2

In Fig. 1a, the pristine VO_2 nanoparticles prepared through a hydrothermal method at 260 °C for 6 h were indexed to VO_2 (M1) (JCPDS No.:72-0514) without other impure phases. The phase transition temperature is 65.1 °C (Fig. 1b), which is slightly lower than the corresponding transition temperature for bulk VO_2 (68 °C). To the best of our knowledge, the post annealing has been widely used to transform other phases (A, B, D) of VO_2 into VO_2 (M1)[20-22]. In addition, a series of phase transition behaviors have been discovered for the VO_2 (A, B, D) nanoparticles, depending on the post annealing conditions. However the thermal treatment just for VO_2 (M1) nanoparticles has not been studied yet. Here we focused on the thermal treatment for pristine VO_2 (M1) nanoparticles. The novel phase transition behaviors will be discussed as follow.

The thermal treatment was carried out in a tube furnace under a flow of nitrogen gas at 400 °C to investigate the effect of annealing time. After annealing for 6h, 12h, 24h, 48h respectively, VO_2 (M1) keeps the monoclinic phase without obvious change and only some weak peaks of V_3O_7 appear in Fig. 1a. It indicates that a bit of VO_2 (M1) is oxidized to V_3O_7 rather than V_2O_5 at high temperatures in N_2 atmosphere. As is well known, the thermal treatment can effectively improve the crystallinity of metal oxide, accompanying with the grain growth and the reduction of point defects. Thus the (011) peak of VO_2 (M1) gradually increases when heating from 0 h to 24 h, but abnormally decreases when heating for 48 h. It can be well explained by the serious oxidation of VO_2, which is verified by the obvious increase of the peaks of V_3O_7 in Fig. 1a.

The phase transition behaviors of annealed VO_2 nanoparticles were characterized by DSC in Fig. 1b and the DSC curves were operated with peak-fit processing via Gaussian fitting method. It is amazing that the DSC curve emerges two peaks and the latent heat of metal–insulator transition (ΔH) noticeably enhances after annealing in

Table 1. A single T_{MIT} of pristine VO_2 (M1) nanoparticles splits into two T_{MIT} and the two T_{MIT} both overtop 65.1 °C. The T_1 is located around 74 °C without obvious fluctuation when the annealing time ranges from 6 to 48 h; while the ΔH_1 (corresponding to the peak at low temperatures) gradually decreases from 23.9 to 11.2 J/g. Compared to T_1, the T_2 is located around 84 °C. The ΔH_2 (corresponding to the peak at high temperatures) increases from 16.2 to 19.7 J/g, opposing with the change of the ΔH_1. It is an extraordinary and interesting phenomenon in the MIT behaviors of VO_2.

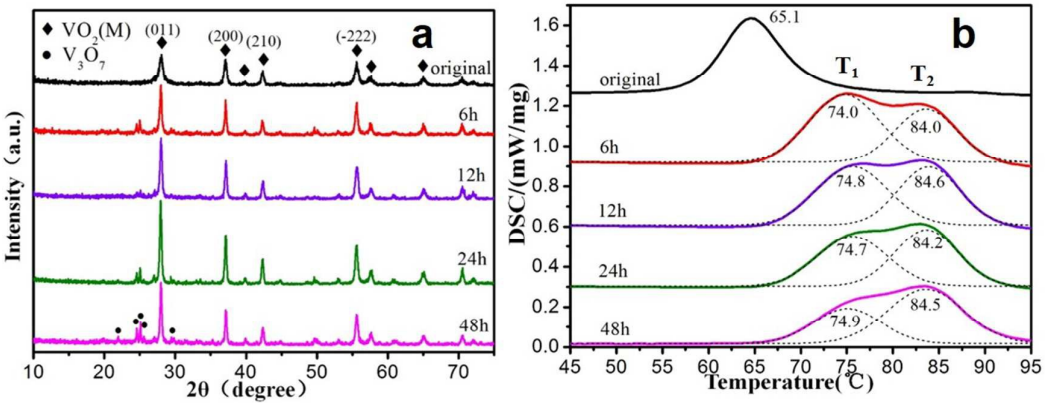

Fig. 1 (a) XRD patterns and (b) DSC curves of VO_2 nanoparticles after annealing at 400 °C for different time; the dashed lines were got via Gaussian fitting method to study the different peaks.

Table. 1 The properties of T_{MIT} and ΔH of the pristine VO_2 and the VO_2 after annealing at 400 °C for different time.

Sample	T_1 (°C)	T_2 (°C)	ΔH_1 (J/g)	ΔH_2 (J/g)	$\Delta H = \Delta H_1 + \Delta H_2$	$\Delta H_1/\Delta H_2$
Pristine VO_2 (M)	T_{MIT} = 65.1 °C		/	/	21.7	/
400 °C – 6 h	74.0	84.0	23.9	16.2	40.1	1.474
400 °C – 12 h	74.8	84.6	21.3	18.1	39.5	1.174
400 °C – 24 h	74.7	84.2	18.2	18.5	36.7	0.984
400 °C – 48 h	74.9	84.2	11.2	19.7	30.9	0.565

Then, the effect of annealing temperatures on MIT of VO_2 was also investigated. Similar phenomena were also found when annealing for 6 h in the range of 400 – 440 °C. In Fig. 2a, as the annealing temperature increases from 400 to 440 °C, the samples remain M1 phase and the (011) peaks of VO_2 (M1) become more intense due to the increase of the crystallinity of VO_2 nanoparticles. In Fig. 2b, a single T_{MIT} (65.1 °C) also splits into two T_{MIT}, which are both above 65.1 °C. T_1 increases from 74.0 to 76.2 °C and T_2 decreases from 84.0 to 82.4 °C when the annealing temperature increases from 400 to 440 °C. Meanwhile, the ΔH_1 decreases from 23.9 to 11.4 J/g and the ΔH_2 increases from 16.2 to 23.3 J/g, as shown in Table 2. We can also find a tendency that T_1 and T_2 peaks gradually merge with the improvement of annealing temperature in Fig. 2b. It seems like the two T_{MIT} peaks combine into one T_{MIT} peak (82.0 °C). In summary, the MIT temperatures of VO_2 would divide into two higher transition temperatures than 65.1 °C when the VO_2 samples are annealed at high temperatures.

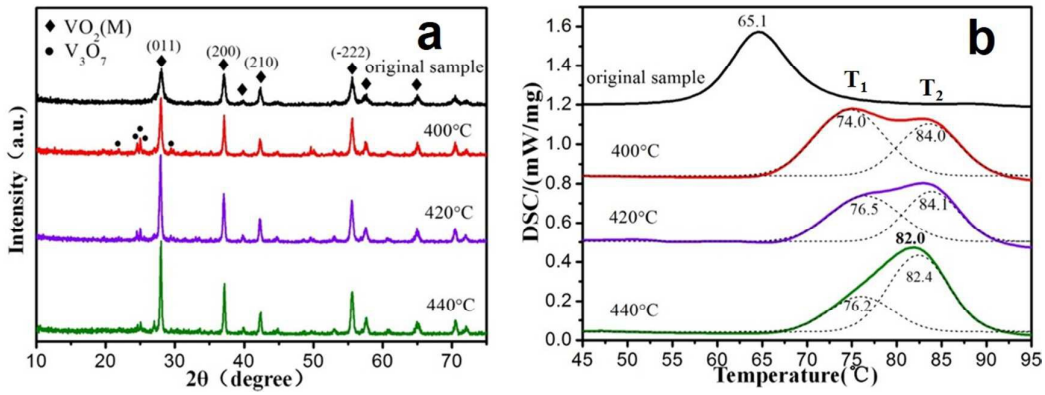

Fig. 2 (a) XRD patterns and (b) DSC curves of VO_2 nanoparticles after annealing at different temperature for 6h; the dashed lines were got via Gaussian fitting method to study the different peaks.

Table. 2 The properties of T_{MIT} and ΔH of the pristine VO_2 and the VO_2 after annealing at different temperature for 6h.

Sample	T_1 (°C)	T_2 (°C)	ΔH_1	ΔH_2 (J/g)	$\Delta H = \Delta H_1 +$	$\Delta H_1/\Delta H_2$

			(J/g)		ΔH_2	
Pristine VO_2 (M)	T_{MIT} = 65.1 °C		/	/	21.7	/
400 °C – 6 h	74.8	84.6	23.9	16.2	40.1	1.474
420 °C – 6 h	76.5	84.1	18.5	15.8	34.4	1.175
440 °C – 6 h	76.2	82.4	11.4	23.3	34.7	0.488

3.2 The mechanism for the novel transition behaviour of VO_2

According to the previous studies, the influence of phase transition temperature could be attributed to a series of effects, including defects, the size effects, and the crystallinity[13, 18, 20, 23]. According to the above findings, when the annealing time and temperature increase, the small nanoparticles merge and grow into large ones. Thereupon the particle size enlarges, the point defect concentration reduces and the VO_2 crystallinity strengthens. In terms of a heterogeneous nucleation process for VO_2, the phase transition depends on the availability of a suitable nucleating defect in the sample space.[24] Thus a higher T_{MIT} induced by a reduced number of defects in the pristine VO_2 nanoparticles will be realized via the thermal treatment. However, the transition temperature of single crystal bulk VO_2 is 68 °C. In any event, the increase of T_{MIT} of VO_2 cannot exceed 68 °C, let alone reach 74 °C and 84 °C. Therefore, it is hard to explain our observed phenomenon of two increasing transition temperatures by these factors.

However, the formation and properties of another monoclinic phase (M2) of VO_2 in VO_2-based strain sensors and actuators were uncovered by Wang et. al and Wu et. al respectively.[14, 15, 25] The M2 phase with a high transition temperature (> 68 °C) under the effect of stress and strain could be interpreted as an intermediate and transitional phase between M1 and R phase[26]. Under tensile strain, the high transition temperature is derived from an insulator (M1) – insulator (M2) phase transition before the insulator (M1) – metal (R) phase transition. But for VO_2 nanoparticles, the elusive M2 phase is almost impossible to be measured and characterized in a single VO_2 particle

with few tens of nanometers. Therefore, the Raman spectra for VO_2 samples were measured to record the phase transition change of VO_2 nanoparticles. For pristine VO_2 samples, the feature peaks at 190, 222, 310, 387, 610 cm^{-1} denoted by blue dash lines can be ascribed to the vibration modes in VO_2 (M1)[5] in Fig. 3a. For VO_2 nanoparticles prepared by annealing at 400 °C for 6h, except for feature peaks of the M1 phase, the peak at 645 cm^{-1} corresponding to the M2 phase found in Fig. 3b. In other words, the annealed VO_2 nanoparticles have a M1 – M2 – R transition during the heating process. The arising of M2 phase is always caused by the generation of stress and strain during annealing at high temperatures, resulting in the abnormal increase of transition temperatures. And in the heating range from 70 to 90 °C, the M1 and M2 phase coexist in Fig.3b. It is obvious that T_1 peak around 74 °C corresponds to the temperature region from 70 to 80 °C and T_2 peak around 84 °C corresponds to the temperature region from 80 to 90 °C in Fig. 3b. Therefore, when heating from 70 to 80 °C, one part of VO_2 has the M1 – M2 – R phase transition and the other part still remains unchanged; while heating up to above 80 °C, the rest VO_2 (M1) also experiences the M1 – M2 – R phase transition, indicating the thermally treated VO_2 (M1) sample holds two different states. Consequently two high and different phase transition temperatures are observed in the VO_2 (M1) samples.

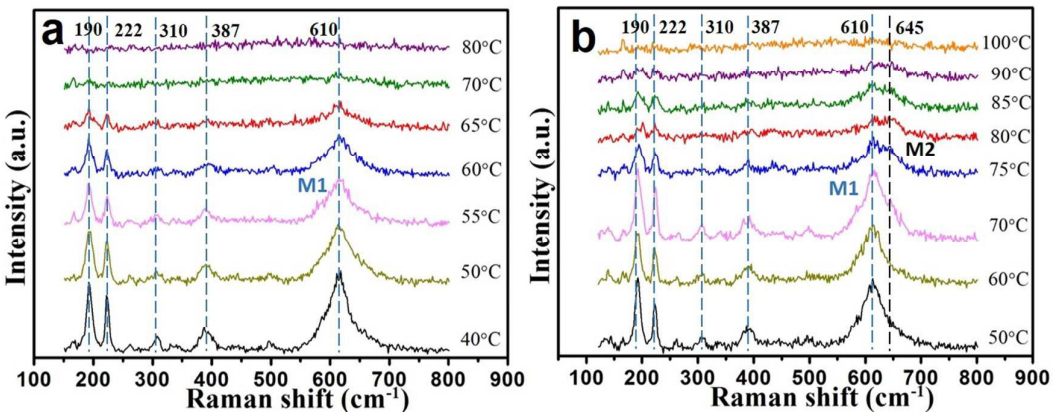

Fig. 3 Characteristic Raman spectra for pristine VO_2 nanoparticles and the VO_2 nanoparticles after annealing at 400 °C for 24 h.

3.3 The morphologies of the annealed VO_2 nanoparticles

Fig. 4 shows the SEM images of pristine and annealed VO_2 nanoparticles. The pristine samples (Fig. 4a) are agglomerative VO_2 nanoparticles with the size of approximately 35 nm and the vague surface seems to be surrounded by amorphous substances with quantities of defects. After annealing at 400 °C for different periods (Fig. 4b – d), the amorphous substances gradually disappear from the surface and the nanoparticles show sharp outlines. It is possibly caused by the recrystallization of VO_2 nanoparticles, and the merging of small particles and further growing into large ones. Thus the particle size gradually increases from 35 nm to 100 nm with the annealing time changing from 0 to 48 h. In Fig. 4d, the fusion of small particles can be clearly seen in the red circle. Naturally it will produce many grain boundaries and dislocation defects during the fusion process. Likewise, the similar merger and growth of small nanoparticles occur at a higher annealing temperature (440 °C) and the shape boundaries are also obvious in Fig. 5.

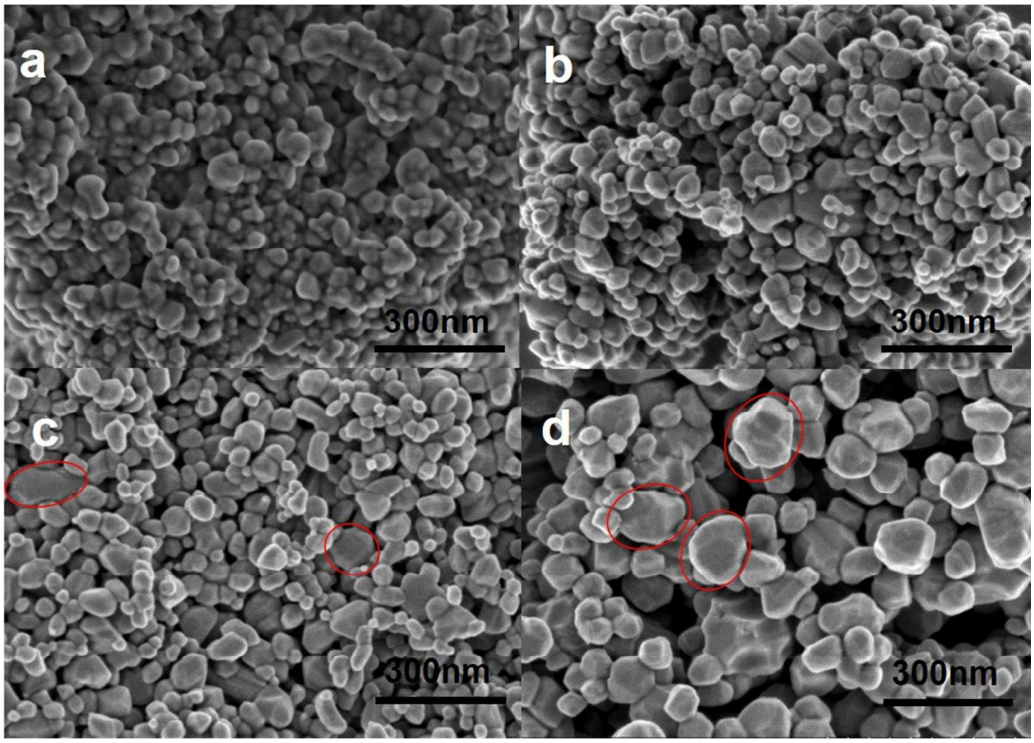

Fig. 4 The SEM images of VO_2 nanoparticles after annealing at 400 °C for (a) 0h; (b) 6h; (c) 12h; and (d) 48h.

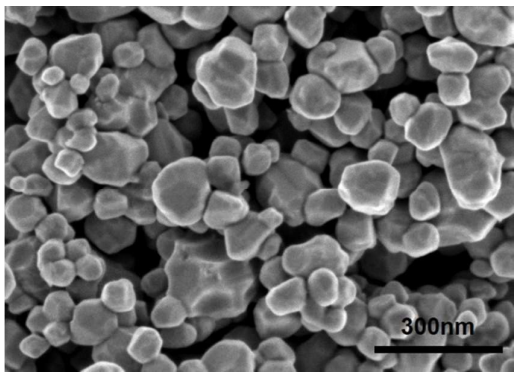

Fig. 5 The SEM images of VO_2 nanoparticles after annealing at 440 °C for 6h.

The TEM analyses also clearly reveal the crystallographic merger and fusion for VO_2 nanoparticles. Fig. 6a shows the pristine VO_2 nanoparticles around 35 nm and the large ones are possibly the reunion of small particles. Then the VO_2 nanoparticles grow larger to 100 nm (Fig. 6b – d) after annealing. However, the fusion process of grain boundaries between two particles can be found in the blue circles in Fig. 6b – d. Specifically the agglomerative VO_2 nanoparticles (Fig. 4a) surrounded with amorphous substances connect together and arrange closely. Annealing at high temperatures, the amorphous substances recrystallize, leading to the merger of two adjacent particles. If the interface between the two particles has the different crystal orientation or a lattice misfit, a grain boundary will be produced naturally. Accompanied by the generation of interfacial defects, the particles will produce stress and strain due to the dislocation of lattice between two particles. We can find a large VO_2 particle combined with several small particles in Fig. 6e and two particles arranges closely and combine together (Fig. 6f).

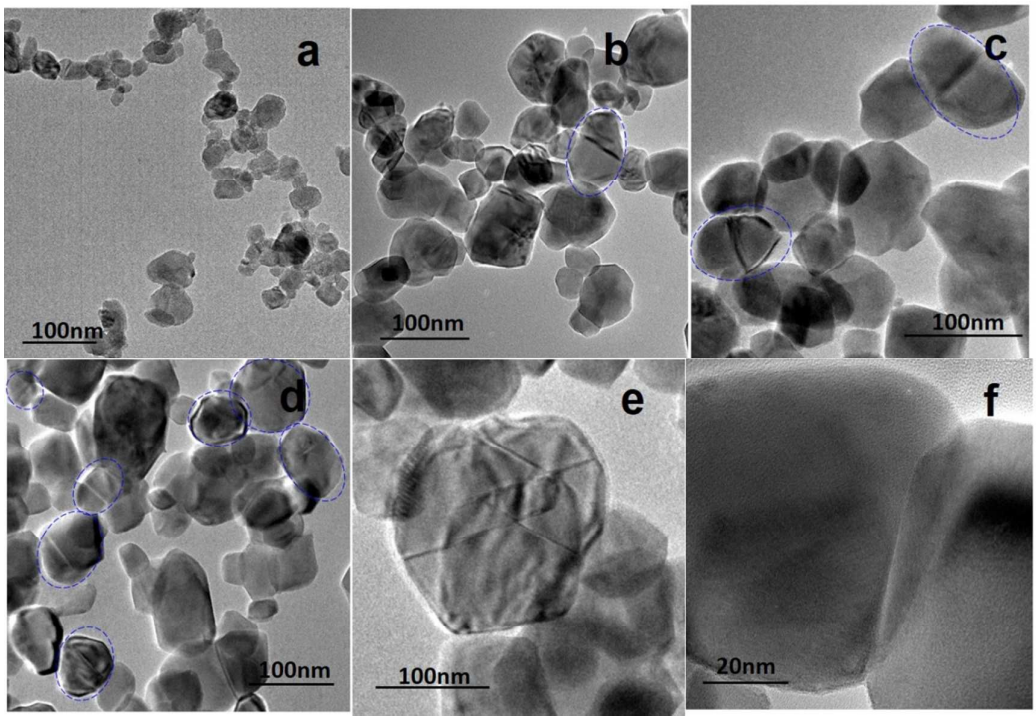

Fig. 6 The TEM images of VO_2 nanoparticles after annealing at 400 °C for (a) 0h; (b) 6h; (c) 12h; (d) 48h; (e) 48h; and (f) 48h.

To further reveal the detailed structural changes of grain boundaries, the high-resolution TEM images and the selected area electron diffraction (SAED) pattern of the annealed VO_2 nanoparticles are shown in Fig. 7. The lattice dislocations between two particles can be clearly observed in Fig. 7a – d. Fig. 7a shows a twin boundary with the lattice misfit in the (200) lattice plane and a misfit angle of 44.8°. The yellow part (above the boundary) and the blue part (below the boundary) have the same [011] zone axis in a monoclinic phase and grow along the (011) preferential direction. The interplanar spacing is calculated to be 0.312 nm, which is indexed as the (011) facet of VO_2 (M1). The corresponding diffraction pattern (the inset in Fig. 7a) obtained by Fourier transform of the HRTEM lattice including the twin boundary presents two lattices. They both have the same structural orientation. And the interplanar spacing characterized in Fig. 7a – c are 0.312, 0.311 and 0.309 nm, respectively. They are slightly smaller than the (011) interplanar spacing (3.2 nm) of normal VO_2 (M1). It means that there is an extra stress and strain along the tetragonal

a-axis of M1 phase. The strain values determined by $\varepsilon = (d_{standard} - d) / d_{standard}$ are 2.5%, 2.28% and 3.13%, respectively, which is large enough to drive the M1 – M2 – R transition behavior and to further raise the transition temperature. Therefore a higher transition temperature will be presented compared to pristine nanoparticles.

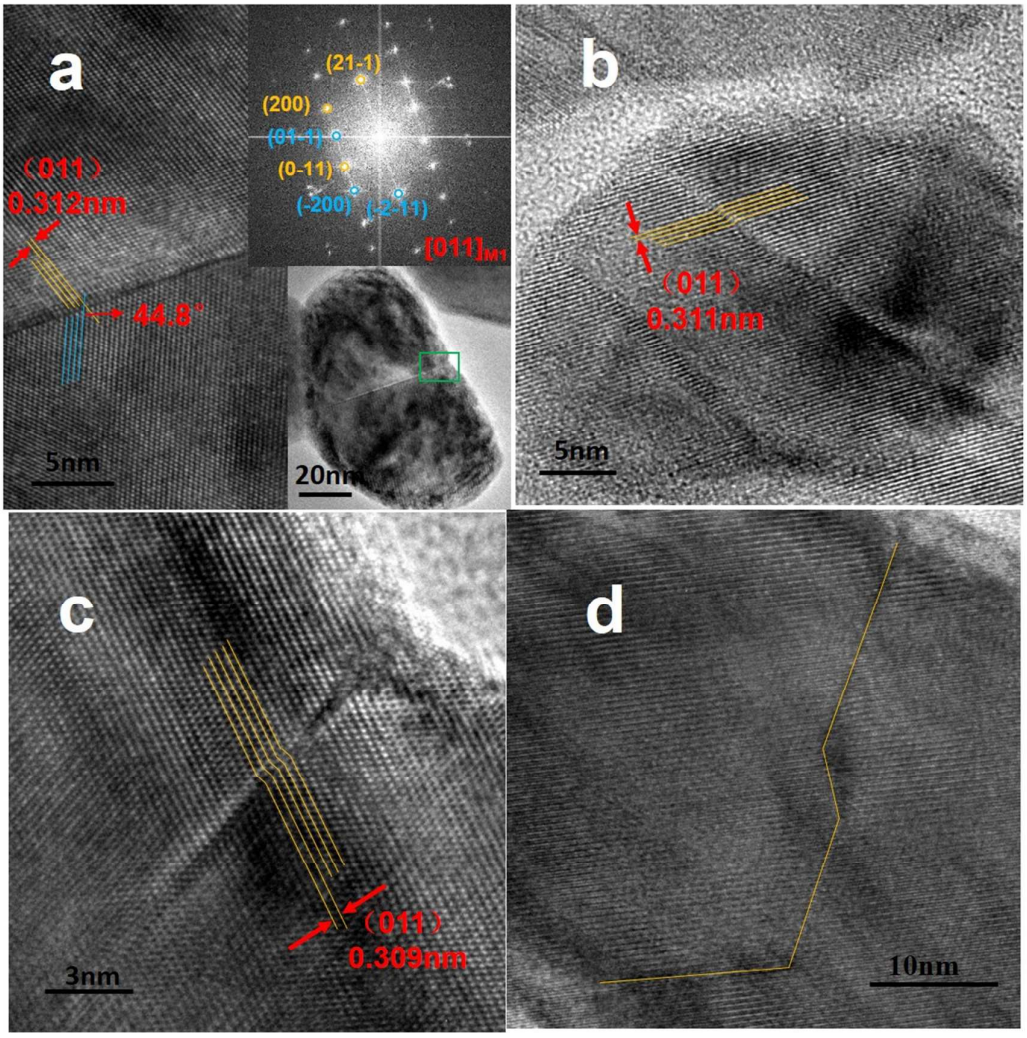

Fig. 7 the SAED and lattice-resolved HRTEM images of the boundaries of annealed VO_2 nanoparticles at 400 °C for (a) 6h; (c) 12h; (d) 48h; and (e)48h.

Through the above characterizations including DSC, Raman spectra, SEM and TEM, two increased transition temperatures (T_1 and T_2) can be further explained clearly as follows: During the grain growth of VO_2 nanoparticles, grain boundaries will generate spontaneously and also can be eliminated by dislocation movement and lattice rearrangement. Hence, the stress with different magnitudes exists on VO_2

nanoparticles. For the T_2 (corresponding to the incompletely grown VO_2 nanoparticles), the stress and strain caused by grain boundaries lead to a M1 – M2 – R behavior and greatly increase the transition temperature to around 84 °C. But for the T_1 (corresponding to the completely grown VO_2 nanoparticles), although the grain boundaries disappear via lattice rearrangement, the residual stress still exists in the VO_2 nanoparticles and is smaller than the stress induced by grain boundaries. Therefore T_1 (74 °C) is lower than T_2 (84 °C), but slightly larger than 68 °C for bulk VO_2.

Moreover, since the ΔH_1 and ΔH_2 correlate to VO_2 nanoparticles without and with grain boundaries, the $\Delta H1/\Delta H2$ reveals the proportion of each part of VO_2 nanoparticles. The dates of ΔH_1 and ΔH_2 in Table 1 and 2 are summarized in Fig. 8a and 8b. We can find that the value of $\Delta H_1/\Delta H_2$ decreases from 1.474 to 0.565 with annealing from 6 to 48 h at 400 °C and decreases from 1.474 to 0.488 with increasing annealing temperature from 400 to 440 °C for 6 h. It indicates that the smaller$\Delta H_1/\Delta H_2$ means the production of more VO_2 nanoparticles with grain boundaries. Likewise, from the SEM and TEM images of Fig. 4a – 4d and Fig. 5a – 5d, the number of VO_2 nanoparticles with grain boundaries in blue circles obviously increases with increasing annealing time. It reveals that the merger of VO_2 nanoparticles with grain boundaries occupies the dominance with the increased annealing temperatures or time.

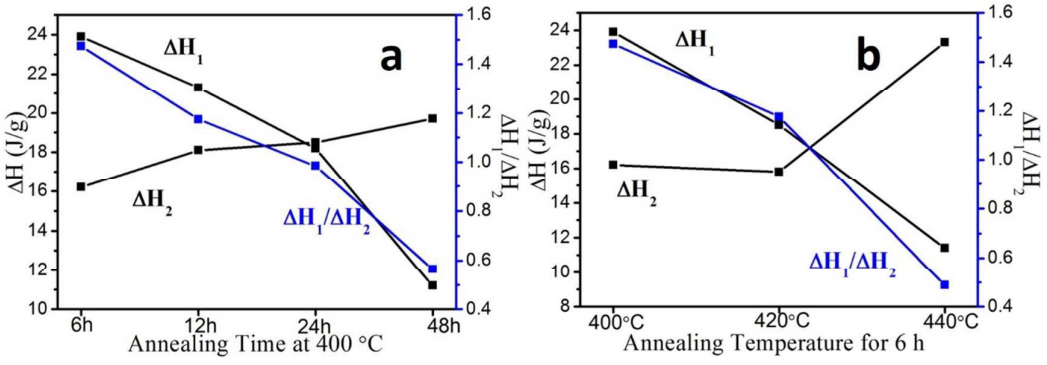

Fig. 8 the correlations of the ΔH_1 and ΔH_2 of the annealed VO_2 nanoparticles.

3.5 The optical property of the annealed VO_2 nanoparticles

Fig. 9a and Table 3 show the variation in the optical and thermochromic properties of the VO_2-PET composite films for different annealing condition. The VO_2 solid content and the film thickness of these foils are fixed. The composite film prepared by pristine VO_2 nanoparticles exhibits a solar modulation ability (ΔT_{sol}) of 12.8% and luminous transmittances (T_{lum}) of 50.5% at 20 ℃ and 48.4% at 100 ℃. But for the annealed VO_2 nanoparticles, the ΔT_{sol} significantly improves without the expense of the T_{lum} value. The T_{lum} value slightly increases to 51.0 – 52.2 % at 20 ℃ and 48.5 – 49.5 % at 25 ℃ after annealing. The transmittance of annealed VO_2 is much lower than the transmittance of pristine VO_2 at 900 –2600 nm in Fig. 9a. The solar transmittance (T_{sol}) at 100 ℃ decrease from 45.9 % to 40.9 – 41.7 %, while the T_{sol} at 20 ℃ remains fairly stable. So the ΔT_{sol} significantly increases from 12.8 % to 15.2 – 17.0 %. The phase transition enthalpy (ΔH) increased from 21.7 J/g to 36.7 – 40.1 J/g after thermal treatment (see Table 1). Thus, the ΔT_{sol} and the ΔH of VO_2 has a positive correlation in Fig. 9b. Therefore, the thermal treatment can improve the solar modulation ability without the expense of the luminous transmittance.

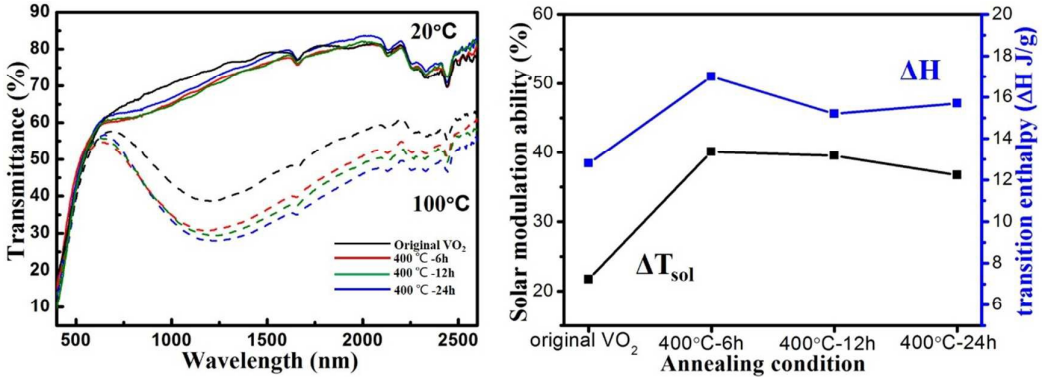

Fig. 9 (a) The transmittance spectra of VO_2-PET composite films at 20 and 90 ℃ for different annealing condition; (b) the relation of the solar modulation ability (ΔT_{sol}) and the phase transition enthalpy (ΔH).

Table 3 The solar energy control properties of VO_2-PET composite films for different annealing condition.

Annealing condition	T_{lum}(%)	T_{sol}(%)	ΔT_{sol}(%)

	20°C	100°C	20°C	100°C	
Pristine VO_2	50.5	48.4	58.6	45.9	12.8
400 °C – 6 h	51.7	48.8	57.8	40.9	17.0
400 °C – 12 h	51.0	49.5	56.6	41.4	15.2
400 °C – 24 h	52.2	48.5	57.4	41.7	15.7

4 Conclusions

An abnormal phase transition process of VO_2 nanoparticles was discovered according to the comparison of pristine nanoparticles without and with high-temperature thermal treatment. One transition temperature (Tc = 65.1 °C) of pristine VO_2 nanoparticles splits into two transition temperatures (T_1 around 74 °C and T_2 around 84 °C). T_2 is corresponding to one part of VO_2 nanoparticles containing grain boundaries. The grain boundaries induced by the merger and fusion of VO_2 nanoparticles at high temperature lead to the generation of stress and strain for VO_2 nanoparticles, hence resulting in a M1 – M2 – R transition behavior of VO_2. Relatively, T_1 is corresponding to the other part of complete grown VO_2 nanoparticles and the residual stress still remain after merger and fusion. Thus the two transition temperatures increase notably and the T_1 is lower than the T_2. Meanwhile, the solar modulation ability (ΔT_{sol}) of VO_2-PET composite film increases from 12.8 % to 15.2 – 17.0 % and the luminous transmittance (T_{lum}) at 20 °C slightly increases from 50.5 % to 51.0 – 52.2 %. This study could enhance the understanding of the MIT of VO_2 nanoparticles and promote the development of VO_2-PET flexible foil.

Acknowledgements

This study was supported in part by funds from MOST (2014AA032802), NSFC (State Outstanding Young Scholars, 51325203) and Shanghai Municipal Science and Technology Commission (15XD1501700).

References

1. F. J. Morin, *Phys. Rev. Lett*, 1959, **34-36**, 34-36.
2. Y. Gao, C. Cao, L. Dai, H. Luo, M. Kanehira, Y. Ding and Z. L. Wang, *Energy Environ. Sci.*, 2012, **5**, 8708.
3. Y. F. Gao, H. J. Luo, Z. T. Zhang, L. T. Kang, Z. Chen, J. Du, M. Kanehira and C. X. Cao, *Nano Energy*, 2012, **1**, 221-246.
4. S. Hormoz and S. Ramanathan, *Solid State Electron.*, 2010, **54**, 654-659.
5. B. Hu, Y. Ding, W. Chen, D. Kulkarni, Y. Shen, V. V. Tsukruk and Z. L. Wang, *Adv. Mater.*, 2010, **22**, 5134-5139.
6. E. Strelcov, Y. Lilach and A. Kolmakov, *Nano Lett.*, 2009.
7. S. Lee, C. Cheng, H. Guo, K. Hippalgaonkar, K. Wang, J. Suh, K. Liu and J. Wu, *J. Am. Chem. Soc.*, 2013, **135**, 4850-4855.
8. J. Cao, W. Fan, Q. Zhou, E. Sheu, A. Liu, C. Barrett and J. Wu, *J. Appl. Phys.*, 2010, **108**, 083538.
9. X. G. Tan, T. Yao, R. Long, Z. H. Sun, Y. J. Feng, H. Cheng, X. Yuan, W. Q. Zhang, Q. H. Liu, C. Z. Wu, Y. Xie and S. Q. Wei, *Sci. Rep.*, 2012, **2**.
10. T. J. Hanlon, J. A. Coath and M. A. Richardson, *Thin Solid Films*, 2003, **436**, 269-272.
11. J. Zhou, Y. Gao, X. Liu, Z. Chen, L. Dai, C. Cao, H. Luo, M. Kanahira, C. Sun and L. Yan, *Phys. Chem. Chem. Phys*, 2013, **15**, 7505-7511.
12. L. Dai, S. Chen, J. Liu, Y. Gao, J. Zhou, Z. Chen, C. Cao, H. Luo and M. Kanehira, *Phys. Chem. Chem. Phys.,* 2013, **15**, 11723
13. L. Dai, C. Cao, Y. Gao and H. Luo, *Sol. Energ. Mat. Sol. C.*, 2011, **95**, 712-715.
14. H. Guo, K. Chen, Y. Oh, K. Wang, C. Dejoie, S. A. Syed Asif, O. L. Warren, Z. W. Shan, J. Wu and A. M. Minor, *Nano Lett*, 2011, **11**, 3207-3213.
15. K. Wang, C. Cheng, E. Cardona, J. Y. Guan, K. Liu and J. Q. Wu, *Acs Nano*, 2013, **7**, 2266-2272.
16. J. Jeong, N. Aetukuri, T. Graf, T. D. Schladt, M. G. Samant and S. S. Parkin, *Science*, 2013, **339**, 1402-1405.
17. M. H. Lee and M. G. Kim, *Thin Solid Films*, 1996, **286**, 219-222.
18. Z. Lu, C. Li and Y. Yin, *J. Mater. Chem.*, 2011, **21**, 14776.
19. Z. Chen, Y. Gao, L. Kang, C. Cao, S. Chen and H. Luo, *J. Mater. Chem. A*, 2014, **2**, 2718.
20. M. Li, X. Wu, L. Li, Y. Wang, D. Li, J. Pan, S. Li, L. Sun and G. Li, *J. Mater. Chem. A*, 2014, **2**, 4520.
21. Y. Zhang, M. Fan, F. Niu, Y. Zhong, C. Huang, X. Liu, B. Wang and H. Li, *Micro Nano Lett.*, 2011, **6**, 888.
22. R. Li, S. Ji, Y. Li, Y. Gao, H. Luo and P. Jin, *Mater. Let.*, 2013, **110**, 241-244.
23. J. Cao, E. Ertekin, V. Srinivasan, W. Fan, S. Huang, H. Zheng, J. W. L. Yim, D. R. Khanal, D. F. Ogletree, J. C. Grossmanan and J. Wu, *Nat. Nanotechnol.*, 2009, **4**, 732-737.
24. R. Lopez, T. E. Haynes, L. A. Boatner, L. C. Feldman and R. F. Haglund, *Phys. Rev. B*, 2002, **65**.
25. J. Cao, W. Fan, K. Chen, N. Tamura, M. Kunz, V. Eyert and J. Wu, *Phys. Rev. B*, 2010, **82**.
26. J. I. Sohn, H. J. Joo, D. Ahn, H. H. Lee, A. E. Porter, K. Kim, D. J. M. Kang and E. Welland, *Nano Lett.*, 2009, **9**, 3392–3397.